

## 15.3 THE EFFECT OF VARIATIONS IN LOW LEVEL THERMODYNAMIC STRUCTURE ON THE REAR FLANK DOWNDRAFT OF SIMULATED SUPERCELLS

Jason Naylor \*

University of North Dakota, Grand Forks, ND

Mark Askelson

University of North Dakota, Grand Forks, ND

### I. INTRODUCTION

Tornadoes remain one of the unsolved mysteries in the atmospheric sciences. They are capable of causing incredible amounts of damage and casualties despite their infrequent occurrence and relatively small spatial scale. A single event, such as the 3 May 1999 outbreak, is capable of producing more than \$1 billion in damage and injuring hundreds of people (Marshall 2002). In order to minimize their impact, it is crucial to gain an understanding of their formation and evolution.

The environmental conditions favorable for supercell formation are well documented (Weisman and Klemp 1986, Rasmussen and Blanchard 1998). Several studies (i.e. Brooks et al. 1994, Thompson et al. 2003, Bunkers et al. 2007) have used observational data to attempt to identify the conditions needed to support supercells that produce significant tornadoes. However, these conditions remain somewhat unclear.

In addition to observations, storm scale models are a useful tool in understanding severe storms. Since their initial development (e.g. Klemp and Wilhelmson 1979), storm scale models have been used extensively to investigate the dynamics of supercells and attempt to understand the origins of low level rotation. Such studies have led to great advancements in our understanding of these systems. However, most of these simulations have utilized simplified microphysics and storm environments. This study examines the sensitivity of low level thermodynamic fields to these simplifications and shows how they relate to current leading theories on tornadogenesis.

#### 1.1 Theories of Tornadogenesis

Pioneering work by Klemp and Rotunno (1983) and Rotunno and Klemp (1985) led to the idea that low level rotation develops in supercells due to the vertical tilting of baroclinically generated horizontal vorticity. Davies-Jones and Brooks (1993) argue that tilting of near-surface horizontal vorticity will not lead to rotation at the

surface. Instead, they suggest that the Rear Flank Downdraft (RFD) is needed to transport high angular momentum air from aloft to the surface while also contributing to tilting and compression of pre-existing vortex lines. This barotropic explanation of tornadogenesis has been alluded to in subsequent studies (e.g., Rasmussen and Straka 2007) and is supported by observations from Markowski et al. (2002). Markowski et al. (2002) found that significant tornadoes were most likely to occur in supercells that had relatively buoyant RFDs. This air can be recirculated back into the updraft where it is stretched and vertical vorticity is intensified. Markowski et al. (2002) concluded that tornadogenesis occurred most frequently in storms where the pseudo-equivalent potential temperature ( $\theta_{ep}$ ) at the surface within the RFD was within 5 K of the  $\theta_{ep}$  found at the surface in the storm environment.

Calculations by both Emanuel (1994) and the authors have shown that thermodynamic processes such as evaporation of rain and melting of ice can only alter  $\theta_{ep}$  values by a few degrees, with evaporation slightly increasing  $\theta_{ep}$  and melting resulting in a small decrease of  $\theta_{ep}$ . Therefore, in order to observe large  $\theta_{ep}$  deficits at the surface, low  $\theta_{ep}$  air must be drawn to the surface from high levels. This theory was validated by Markowski et al. (2002) and by Markowski et al. (2003). Both suggest that tornadic supercells had RFDs with low origin heights while nontornadic supercells were characterized by RFDs with much higher origin levels. The question that has been left unanswered thus far is what environmental conditions influence the origin level of RFDs?

Using a simplified column model, Askelson et al. (2004) performed simulations of downdraft flow in two environments; (1) a conditionally unstable environment with a constant lapse rate throughout and (2) an environment containing a capping inversion just above the boundary layer. The results show that downdrafts formed in the capped environment have lower origin levels and minimize  $\theta_{ep}$  deficits at the surface. In the non-capped environment, downdrafts initially form several kilometers above the surface where evaporative cooling from raindrops and melting of graupel and hail is first experienced. The downdrafts continue to strengthen as they extend to the surface. In the capped environment, downdrafts are stopped in the capped layer owing to negative buoyancy. The

---

\* *Corresponding author address:* Jason Naylor, University of North Dakota, Dept. of Atmospheric Sciences, P.O. Box 9006, Grand Forks, ND 58202  
Email: jason.naylor@und.nodak.edu

precipitation falls through the capped layer and re-excites a new downdraft below the cap.

If a capping inversion does in fact alter the low level thermodynamic structure of a supercell, then it is a critical component of the barotropic tornadogenesis mechanism outlined by Markowski et al. (2002). However, the vast majority of numerical storm simulations do not have a capping inversion in the initial storm environment. This study expands on that of Askelson et al. (2004) by using a more sophisticated, three dimensional model to simulate the low level thermodynamic evolution of supercells created in both a capped and non capped environment.

## 2. METHODOLOGY

Idealized simulations were performed using the Advanced Research WRF (ARW) dynamics core of the Weather Research and Forecasting (WRF) model (Skamarock et al. 2005). All simulations were run on a 600 x 600 x 81 grid for 120 minutes with 250 m grid spacing (both in the horizontal and vertical) using a 1 s time step. Convection was initiated using a 5 K thermal perturbation inserted in the center of the domain. Two temperature profiles similar to those used in Askelson et al. (2004) were used to initialize the models (Figure 1). The first is a conditionally unstable profile (herein referred to as the non-capped profile) that resembles those used in most idealized storm simulations. The second temperature profile, referred to herein as the capped profile, is derived from the first with the addition of a capping inversion from 0.75-1.25 km. In addition, two separate microphysics schemes were employed. The first is a liquid only scheme outlined by Kessler (1969) and the second is a mixed phase scheme developed by Lin et al. (1983) (herein LFO83).

It should be noted that the capped and non-capped temperature profiles have different  $\theta_{ep}$  profiles, with the capped temperature profile having slightly higher  $\theta_{ep}$  values from 0-3 km (Figure 2). Therefore, for this reason alone one could expect higher low level  $\theta_{ep}$  values in the capped simulation. The goal of this study is to determine if the presence of a cap will increase low level  $\theta_{ep}$  values by altering the dynamics of downdrafts and thus this initial bias needs to be considered. Figure 2 shows that the maximum difference in  $\theta_{ep}$  in the 0-3 km layer between the two soundings is approximately 3 K. Hence, in order to conclude that the differences observed in low level  $\theta_{ep}$  values are a result of dynamic interactions with the capped layer, these differences must be larger than 3 K.

The two environments also differ in their potential to produce downdrafts. The capped sounding has Downdraft Convective Available Potential Energy (DCAPE) values that are approximately 140 J kg<sup>-1</sup> higher than the non-capped sounding. This is most likely due to the presence of a layer directly above the

cap with nearly dry adiabatic lapse rate. This layer is needed in order to keep the Convective Available Potential Energy (CAPE) values of the two soundings similar. However, the fact that DCAPE is higher in the capped environment may be troublesome since it is believed that strong downdrafts have the ability to puncture through caps and continue the transport of low  $\theta_{ep}$  air to the surface.

Values within the appendage region of the simulated supercells are the main focus of the analysis. The appendage region is defined as the region within the hook shaped appendage of the 750 m precipitation mixing ratio ( $q_{ra}$  in the Kessler simulations and  $q_{pr}$  in the LFO83 simulations) contours. If no hook shaped appendage is present at a specific time, then values near the updraft are examined. Analysis of the results is focused on the values at 250 m due to the orientation of the vertical grid. This is the lowest level at which temperature and wind values are computed. At all levels below this, temperature values will be extrapolated. Downdrafts at 2.5 km are also analyzed to determine if the differences in low level RFD intensity may be attributed to large differences in downdraft intensity aloft.

## 3. RESULTS

### 3.1 Kessler Microphysics

Both the capped and non-capped environments produce strong, long lived supercells that are similar in size and intensity. There are some differences in their storm motions as the non-capped supercell propagated farther towards the southern boundary. The evolution of the two supercells is comparable, with the capped storm developing supercellular structure slightly earlier. The largest and most intense downdrafts occurred in the non-capped supercell both in the rear and forward flank. The average maximum velocity of the 250 m RFD in the non-capped supercell is greater than the in the capped supercell at every time except 100 min. However at 2.5 km, the average maximum RFD values are very similar. This may be evidence that the downdrafts in the capped supercell are decelerating in the capped layer. After 105 min, the 2.5 km RFD in the non-capped supercell becomes slightly larger and more intense than that of the capped supercell. On average, the differences in the 250 m RFDs are greater than the differences in the 2.5 km RFDs (Table 1).

Differences in the low level  $\theta_{ep}$  fields are present, but may be a result of variances in the temporal evolution of the supercells. In the simulations low-level  $\theta_{ep}$  values fluctuate with time and depend somewhat on the evolutionary phase of the storm.  $\theta_{ep}$  deficits in the RFD region of both supercells tend to be minimized when the hook shaped appendage is most prominent. For this reason, it may be fallacious to compare the two storms

when they are at different points in their evolution. Therefore, the times at which the supercells were most mature (i.e. strong updraft, RFD at low levels and a hook shaped appendage) are compared. Figure 4 illustrates a time at which the supercells were both at a mature state.

Table 1 shows the maximum and minimum  $\theta_{ep}$  deficits observed in the appendage at each time in the study period. There is little variation in the minimum  $\theta_{ep}$  deficits, but the maximum deficits are different. The average maximum  $\theta_{ep}$  deficit is nearly 4 K higher in the non-capped supercell. This difference is even larger when only mature phases of the storms are considered (100 min, 105 min, 120 min for the non-capped supercell and 95 min, 100 min, 115 min, and 120 min for the capped supercell). When the storms are at their most mature state, the average maximum  $\theta_{ep}$  deficit in the non-capped supercell is nearly 12 K, while the average maximum deficit in the capped supercell is 5.75 K. This difference is nearly twice that caused by the addition of a cap. Overall, when the supercells have reached peak maturity, the capped supercell has air with significantly higher  $\theta_{ep}$  in the appendage region than the non-capped supercell.

### 3.2 LFO83 Simulations

As was seen in the Kessler simulations, both the non-capped and capped environments produced strong, long lived supercells with the non-capped supercell again propagating farther towards the southern boundary. One striking difference between the non-capped and capped supercells is the variance in the  $q_{pr}$  fields. At all times in the study period, the 750 m  $q_{pr}$  values in the capped supercell were significantly lower than those in the default supercell. This difference was not evident in the Kessler simulations, so it is believed to be directly related to ice processes. It is unclear exactly what is causing this discrepancy, but it may be related to changes in mid-level relative humidity. Temperatures (mixing ratios) in the capped environment are higher (lower) than in the non-capped environment from 1-3 km. This may have led to additional melting and subsequent evaporation which would decrease  $q_{pr}$  values.

In the LFO83 simulations, the maximum  $\theta_{ep}$  deficits were nearly identical between the non-capped and capped supercells. There was some slight variance in the minimum  $\theta_{ep}$  deficits, however these differences were always less than 3 K and therefore not large enough to be significant. Similar results were obtained when only considering the storms at their peak intensity (Fig. 5). The uniformity in the  $\theta_{ep}$  fields could be a result of increased melting in the capped simulation. As mentioned previously, temperatures are higher in the capped sounding from 1-3 km. The increased melting that would occur in this layer may have contributed to

some larger decreases in  $\theta_{ep}$  than seen in the non-capped environment by forcing stronger downdrafts able to penetrate through the cap. Table 2 shows that the average maximum RFD velocity at 2.5 km is higher in the non-capped supercell, while the average 250 m RFD is actually higher in the capped supercell. This may be evidence that the RFD is accelerating in the cap.

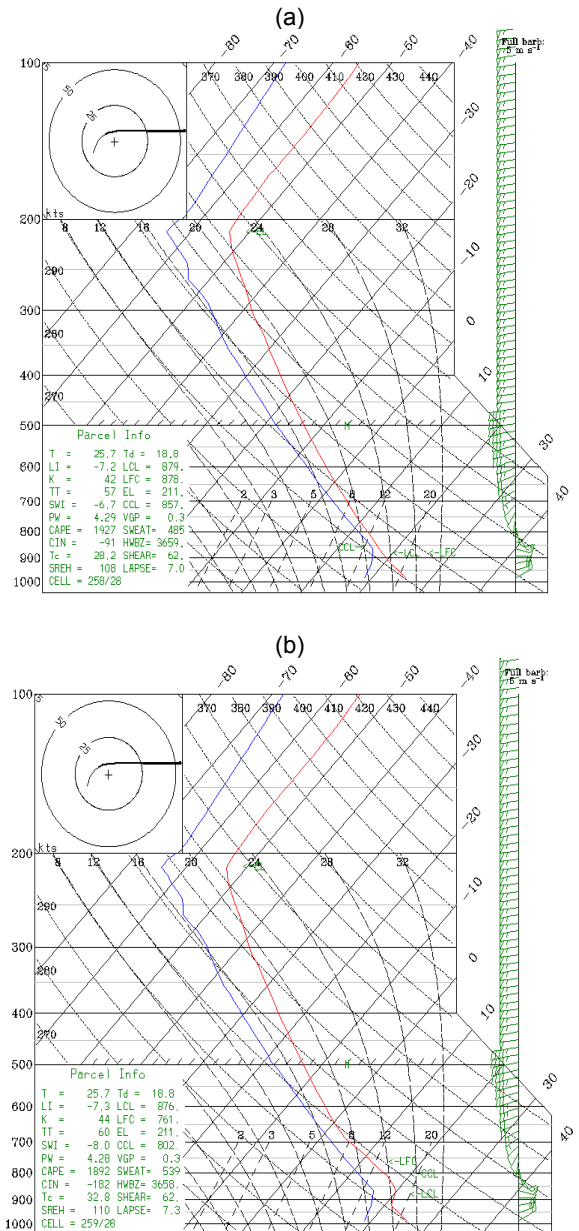


Figure 1: Soundings used to represent storm environments. (a) is the non-capped sounding and (b) is the capped sounding.

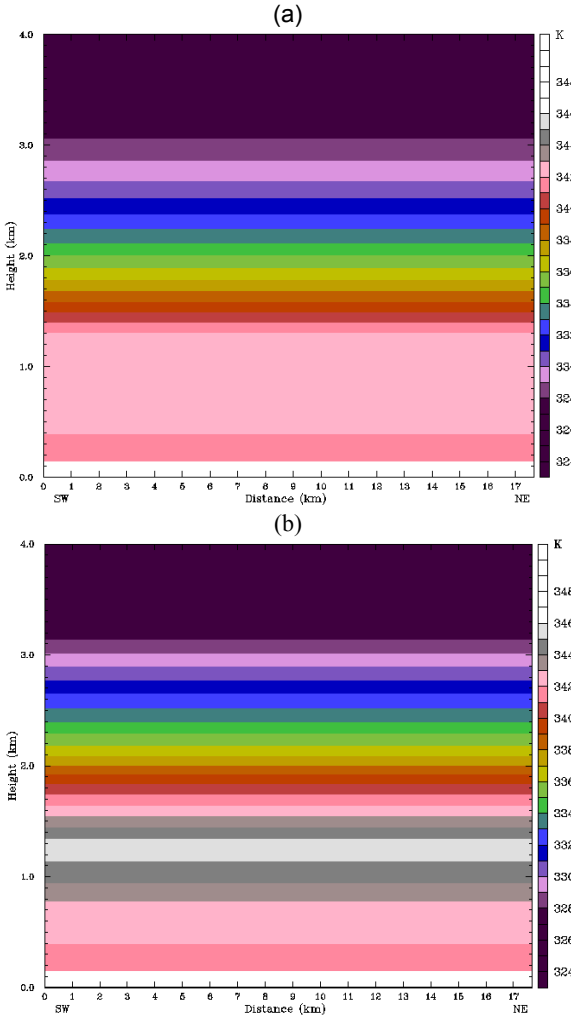


Figure 2: Cross section of  $\theta_{ep}$  from 0-4 km. (a) represents the default environment and (b) represents the capped environment.

#### 4. DISCUSSION

Deficits of  $\theta_{ep}$  in the LFO83 simulations were much larger than the deficits in the Kessler simulations. The largest deficits observed in the appendage of the supercells were 16 K in the Kessler simulations and 18 K in the LFO simulations. However, the occurrence of the large deficits varied greatly. There were only two times in the Kessler simulation where the maximum  $\theta_{ep}$  deficit was greater than 10 K in the default case and no instances where the deficit was greater than 10 K in the capped case. In the LFO simulations, both supercells had maximum  $\theta_{ep}$  deficits greater than 15 K at every time throughout the 90-120 min study period. These differences in low level  $\theta_{ep}$  fields are probably a result of

differences in downdraft production. Stronger downdrafts would be more capable of transporting upper level, low  $\theta_{ep}$  air to the surface. Downdrafts produced in the LFO83 simulations were both larger and stronger at both 250 m and 2.5 km than those produced in the Kessler simulations. At 2.5 km, the strongest downdrafts observed in the LFO83 simulations occurred in the Forward Flank Downdraft (FFD) of the capped supercell at 100 min and topped  $20 \text{ m s}^{-1}$ . The strongest FFD observed in the Kessler simulations was  $16 \text{ m s}^{-1}$ , which was observed in the capped supercell simulation at 105 min. RFDs were similar in magnitude but varied in size. RFDs in the LFO83 simulations tended to be slightly larger and have larger regions of maximum velocity at 250 m.

The cause of these differences in downdraft intensity is believed to be related to melting and evaporation processes. In the Kessler simulations, evaporational cooling is the main thermodynamic process driving downdrafts. However, high relative humidities throughout most of the sounding limited evaporation and downdraft production. The same RH values that were unfavorable for evaporation were preferential for melting processes in the LFO83 simulations. These high RH values enabled large amounts of melting to occur by limiting graupel and hailstone growth through evaporation, resulting in enough cooling to drive strong downdrafts. Downdrafts were slightly stronger in the capped simulations, where relative humidities were lower between 900 and 700 mb (above the cap).

Analysis of low level  $\theta_{ep}$  values throughout the appendage region of the supercells showed that  $\theta_{ep}$  values were significantly higher in the capped supercell when Kessler microphysics were utilized, but not in the simulations using LFO83 microphysics. This is most likely a result of the large, strong downdrafts present in the LFO83 simulations that penetrated through the cap.

The cause of these intense downdrafts is somewhat unclear. It may be possible that fundamental limitations in the microphysical parameterization schemes may be the cause. Both the Kessler and LFO83 schemes are single moment microphysics schemes, meaning that concentration of drops is not predicted, and the drop size distribution is reset to an inverse exponential distribution after each time step. This creates a large number of small droplets at each time step that would not exist in reality. These small drops are easily melted and evaporated in a short amount of time (Srivastava 1985, 1987). Because of their rapid melting and evaporation rates, these small hydrometeors strongly drive downdrafts and, thus, their “false” presence causes unrealistic downdraft forcing. It is believed this effect would be much stronger in the LFO83 simulations because both melting and evaporation are forcing the downdrafts there, while only evaporation is present in the Kessler simulations to force downdrafts.

The downdraft model utilized in Askelson et al. (2004) can be used to test the sensitivity of downdrafts to the presence of small rain drops. The Askelson model uses a bin microphysics scheme that is initialized assuming exponential size distributions for both rain and graupel/hail. Thus, this model does not artificially inject small hydrometeors in areas where they would have completely evaporated. A test was performed that consisted of varying the precipitation release altitude above a capped layer. With a release just above a capped layer, small hydrometeors are still present to enhance downdraft forcing within that layer. With releases further above the capped layer, these small hydrometeors are not available to force downdraft within the capped layer owing to their complete evaporation. The results of the test are shown in Fig. 3. In Fig. 3a, the precipitation is released 200 m above the top of the capped layer, allowing sufficient time for many of the small drops to be evaporated. Once the downdraft impinges upon the cap, the downdraft decelerates and eventually stops, only to be re-excited beneath the cap. In Fig. 3b, the precipitation is released just 100 m lower than in (a), providing slightly less time for the smaller drops to be evaporated before reaching the capped layer. In this scenario, the downdraft never completely stops in the capped layer, suggesting that the presence of small drops is having a strong impact on downdraft evolution and sustenance.

Li et al. (2008) performed a direct comparison between two squall line simulations; one using bin microphysics and the other using a single moment bulk microphysics based on LFO83. Their results showed that the downdrafts in the bin microphysics simulation more accurately represented the downdrafts observed in the storm. The downdrafts in the bulk microphysics simulation were overestimated by nearly 50%. They attributed this to artificially enhanced evaporation rates caused by the use of a fixed precipitation drop size distribution.

The simulations presented in this study have provided some evidence that the cap can have a significant influence on the low level  $\theta_{ep}$  fields. However, it is believed that the results could be strengthened with some improvements in the methodology. Since it is believed that thermodynamics play a vital role in tornadogenesis, it is imperative that the storm environment be as realistic as possible. Also, the use of single moment bulk microphysics schemes likely led to the artificial creation of many small hydrometeors in downdrafts that would not be present in a real world situation. The single moment bulk scheme creates a new drop size distribution after every time step, essentially reinserting many small drops in downdrafts and, thus, providing additional forcing for downdrafts. Evidence was presented to support this hypothesis. It would be worthwhile to revisit this study

with improved microphysics and new input soundings that contain more realistic moisture profiles.

Future work is concentrated mainly on trajectory analysis of the RFD and calculations of scalars along the trajectories. Trajectories will be able to conclusively determine whether or not the differences observed in the low level  $\theta_{ep}$  field are a result of differences in RFD origin height or the result of some other mechanism. Also, calculation of scalars along these trajectories will help to diagnose the degree of microphysically induced cooling of the downdraft air as it descends. This will help determine if the relatively warm capped layer produced a significant increase in melting which may have led to the poor results in the LFO83 simulations.

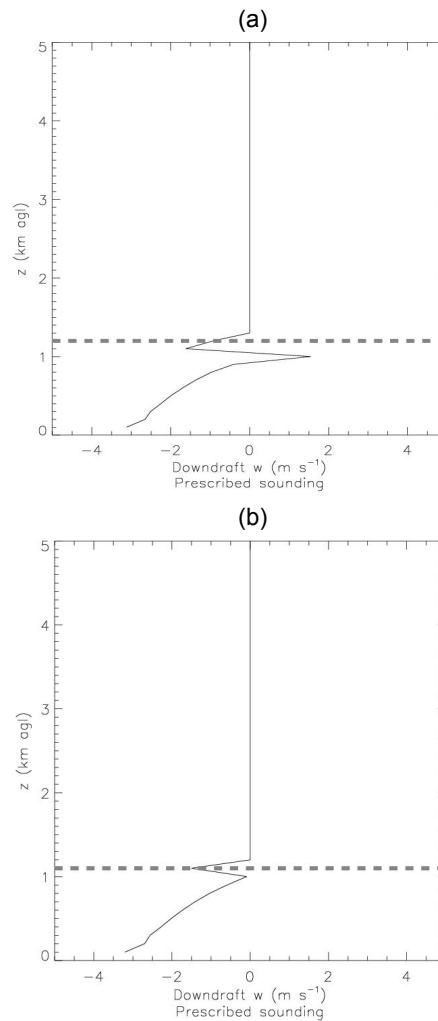


Fig. 3: Results from a test performed using the Askelson et al. (2004) downdraft model for (a) 1.2 km precipitation release altitude and (b) 1.1 km precipitation release altitude. Dashed line indicates height of precipitation release.

Table 1: Summary of  $\theta_{ep}$  deficits throughout the appendage region in the Kessler simulations. (c) indicates the times when the capped supercell was at peak intensity, (n) indicates the time at which the non-capped supercell was at peak intensity and (b) indicates times when both supercells were at peak intensity.

Time	Non-Capped Supercell				Capped Supercell			
	Max $\theta_{ep}$ Deficit	Min $\theta_{ep}$ Deficit	Max RFD 250 m	Max RFD 2.5 km	Max $\theta_{ep}$ Deficit	Min $\theta_{ep}$ Deficit	Max RFD 250 m	Max RFD 2.5 km
<b>90 min</b>	8.0	3.0	3.0	4.0	4.0	0.0	2.5	6.0
<b>95 min (c)</b>	8.0	1.0	3.0	2.0	5.0	0.0	1.5	6.0
<b>100 min (b)</b>	5.0	1.0	3.0	6.0	8.0	1.0	3.0	4.0
<b>105 min (n)</b>	14.0	3.0	3.0	6.0	9.0	1.0	2.0	8.0
<b>110 min</b>	6.0	0.0	4.0	8.0	3.0	1.0	2.0	6.0
<b>115 min (c)</b>	9.0	1.0	3.5	6.0	1.0	0.0	2.5	6.0
<b>120 min (b)</b>	16.0	2.0	3.0	6.0	9.0	-1.0	2.5	4.0
<b>Avg.</b>	<b>9.4</b>	<b>1.6</b>	<b>3.2</b>	<b>5.4</b>	<b>5.6</b>	<b>0.3</b>	<b>2.3</b>	<b>5.7</b>

Table 2: Summary of  $\theta_{ep}$  deficits throughout the appendage region in the LFO83 simulations. (c) indicates the times when the capped supercell was at peak intensity (n) indicates the times that the non-capped supercell was at peak intensity and (b) indicates times when both supercells were at peak intensity

Time	Non-Capped Supercell				Capped Supercell			
	Max $\theta_{ep}$ Deficit	Min $\theta_{ep}$ Deficit	Max RFD 250 m	Max RFD 2.5 km	Max $\theta_{ep}$ Deficit	Min $\theta_{ep}$ Deficit	Max RFD 250 m	Max RFD 2.5 km
<b>90 min (c)</b>	18.0	11.0	2.5	6.0	18.0	7.0	4.5	8.0
<b>95 min (n)</b>	17.0	7.0	4.5	10.0	17.0	9.0	2.5	4.0
<b>100 min (b)</b>	17.0	10.0	2.5	6.0	15.0	7.0	3.5	6.0
<b>105 min (b)</b>	16.0	10.0	2.5	6.0	16.0	9.0	4.0	6.0
<b>110 min (n)</b>	17.0	13.0	2.5	8.0	16.0	7.0	3.0	6.0
<b>115 min</b>	16.0	11.0	3.5	8.0	17.0	11.0	3.0	6.0
<b>120 min</b>	18.0	9.0	4.0	10.0	16.0	6.0	4.0	6.0
<b>Avg.</b>	<b>17.0</b>	<b>10.1</b>	<b>3.2</b>	<b>7.7</b>	<b>16.4</b>	<b>8.0</b>	<b>3.5</b>	<b>6.0</b>

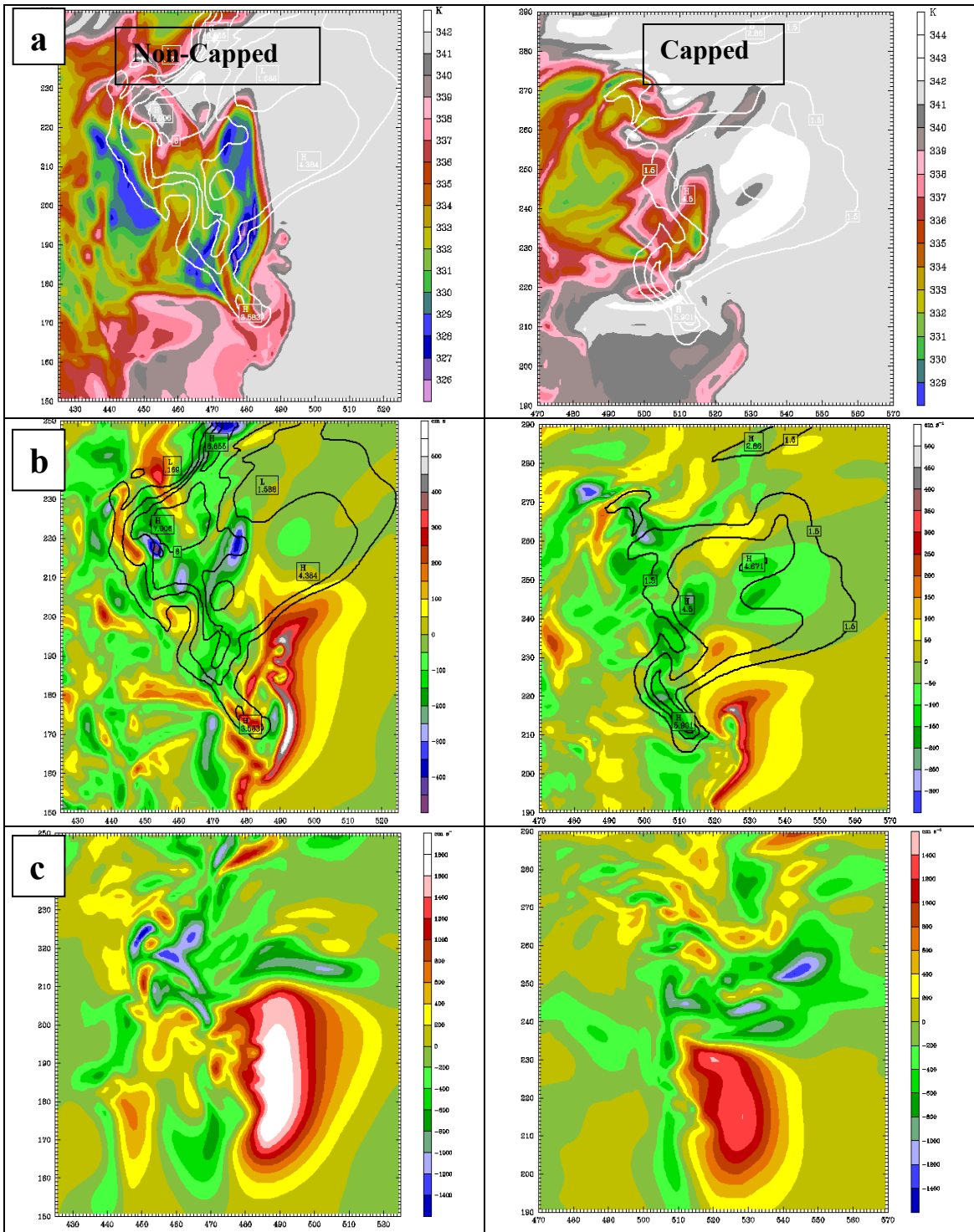


Figure 4: Comparison of simulated supercell characteristics at 120 min using Kessler microphysics. White lines in (a) and black lines in (b) represent rain water mixing ratio at 750 m altitude with a contour interval of  $1 \text{ g kg}^{-1}$ . Colors in (a) are  $\theta_{ep}$  at 250 m. Colors in (b) are vertical velocity at 250 m in units of  $\text{cm s}^{-1}$  and colors in (c) are vertical velocity at 2.5 km, again in  $\text{cm s}^{-1}$ .

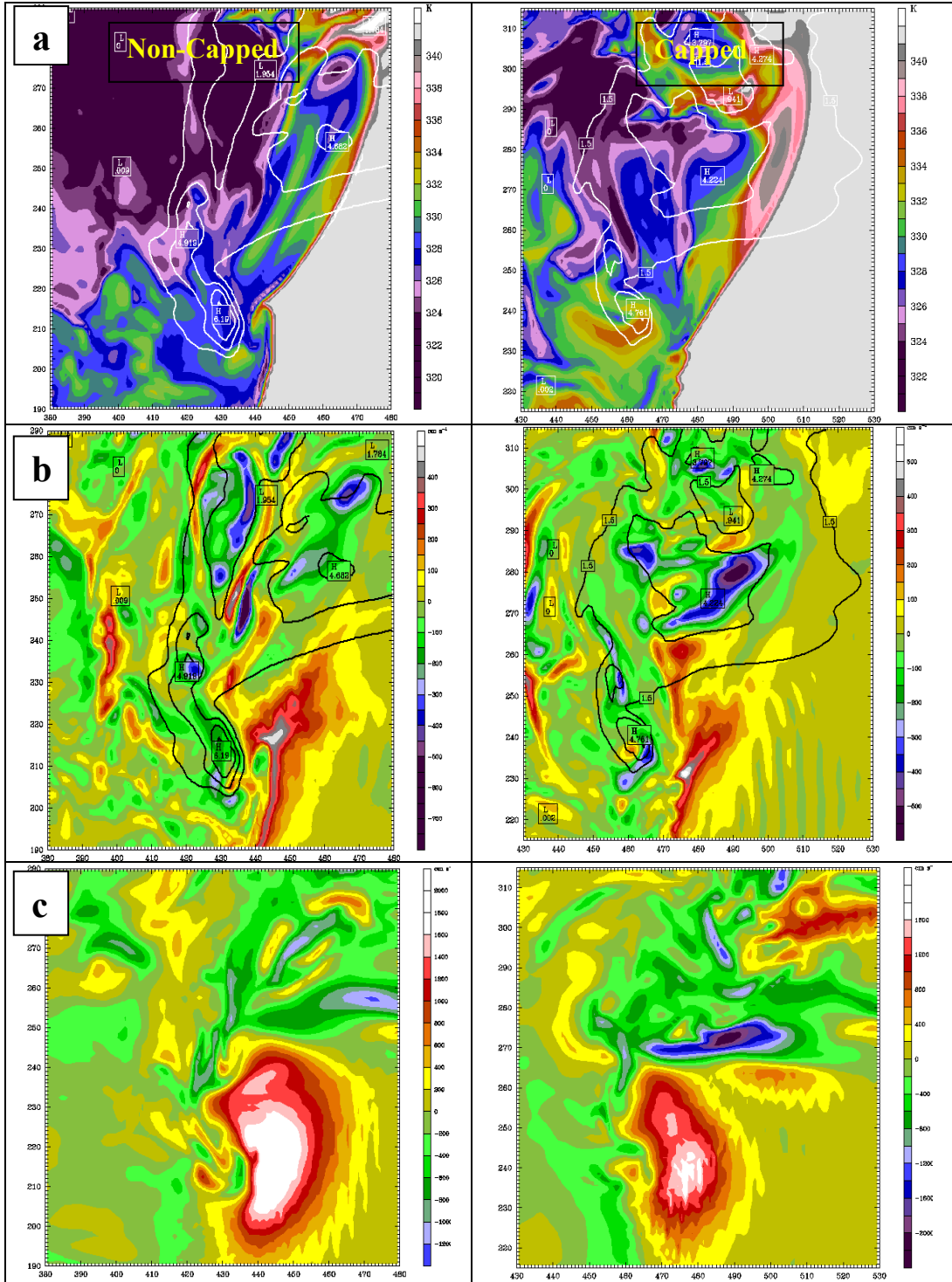


Figure 5: Comparison of simulated supercell characteristics at 100 min using LFO83 microphysics. White lines in (a) and black lines in (b) represent total precipitation mixing ratio at 250 m altitude with a contour interval of  $1 \text{ g kg}^{-1}$ . Colors in (a) are  $\theta_{ep}$  at 250 m. Colors in (b) are vertical velocity at 250 m in units of  $\text{cm s}^{-1}$  and colors in (c) are vertical velocity at 2.5 km, again in  $\text{cm s}^{-1}$ .

## 5. CONCLUSIONS

One of the “behind the scenes” goals of this study was simply to determine if a supercell could be simulated in an environment containing a significant temperature inversion. The results from this portion of the study are summarized below.

- The capped environment was able to support long lived supercells that were comparable to the supercells generated in the non-capped environments. The capped supercells tended to mature slightly faster than the non-capped supercells.
- The non-capped supercells seemed to have stronger rightward propagation, as they were continuously closer to the southern domain boundary than the capped supercells.
- Updrafts were smaller and less intense in the capped environment.
- Downdraft production *potential* was higher in the capped sounding than in the default sounding. DCAPE in the capped sounding is over  $140 \text{ J kg}^{-1}$  larger than in the default sounding.

The main goal of this study was to determine the influence of the cap on low level  $\theta_{ep}$  field as well as analyzing the effects of microphysical parameterizations on  $\theta_{ep}$  values. The following conclusions can be drawn:

- The introduction of a cap into the temperature profile altered the pre-storm  $\theta_{ep}$  field by as much as 3 K. In order to determine if the cap prevents upper level, low  $\theta_{ep}$  air from being transported to the surface, the differences observed at low levels must be greater than this 3 K difference.
- In the Kessler simulations, when the supercells were at their most mature state, the appendage region of the capped supercell had 250 m  $\theta_{ep}$  values that were nearly 6 K higher than the  $\theta_{ep}$  values in the appendage region of the non-capped supercell. There was no significant difference in the appendage region of the supercells when LFO83 microphysics were used. This is most likely a result of the stronger downdrafts in the LFO83 simulations punching through the capped layer.
- Downdrafts tended to be stronger when the LFO83 microphysics scheme was used. In the Kessler simulations, the average maximum 250 m RFD speed was smaller for the capped supercell than for the non-capped supercell. However, in the LFO83 simulations the average maximum 250 m RFD speed was larger in the capped supercell. This is most likely due to the higher temperatures and lower relative humidities in the capped layer that provided additional melting and evaporation. In the LFO83 simulations, these two effects would have

produced additional forcing with the capped sounding that is not present with the non-capped sounding.

- Low level  $\theta_{ep}$  seems to be dependent on the developmental phase of the supercell. Deficits of  $\theta_{ep}$  in the supercells were minimized when the hook shaped appendages were most prominent.

Future work is currently being conducted to answer the following questions:

- What are the origin level of RFDs in the capped supercell and non-capped supercells?
- How much deceleration of the RFD occurs in the capped layer?
- How much cooling due to evaporation and cooling is occurring as the RFD descends to low levels?
- Is there a difference in the amount of microphysically induced cooling that is experienced between the capped and non-capped environments?
- Are the differences between the low level  $\theta_{ep}$  deficits of the Kessler and LFO83 simulations a result of increased cooling due to evaporation and melting?

## ACKNOWLEDGEMENTS

This work was partially sponsored by the National Science Foundation under Grand EPF-0447679.

## REFERENCES

- Askelson, M., J. Straka, and E. Rasmussen, 2004: Precipitation, the rear flank downdraft, and tornadoes. *22<sup>nd</sup> Conf. on Severe Local Storms*, Hyannis, MA, Amer. Meteor. Soc.
- Brooks, H. E., C. A. Doswell III, and R. Davies-Jones, 1993: Environmental helicity and the maintenance and evolution of low-level mesocyclones. *The Tornado: Its Structure, Dynamics, Prediction, and Hazards, Geophys. Monogr.*, No 79, Amer. Geophys. Union, 97-104.
- \_\_\_\_\_, \_\_\_\_\_, J. Cooper, 1994: On the environments of tornadic and nontornadic mesocyclones. *Wea. Forecasting*, **9**, 606-618.
- Bunkers, M. J., J. S. Johnson, L. J. Czepyha, J. M. Grzywacz, B. A. Klimowski, M. R. Hjelmfelt, 2006: An observational examination of long-lived supercells. Part II: Environmental conditions and forecasting. *Wea. Forecasting*, **21**, 689-714.

- Davies-Jones, R., 1984: Streamwise vorticity: The origin of updraft rotation in supercell storms. *J. Atmos. Sci.* **41**, 2991-3006.
- \_\_\_\_\_, 2002: Linear and nonlinear propagation of supercell storms. *J. Atmos. Sci.*, **59**, 3178-3205.
- \_\_\_\_\_, and H. Brooks, 1993: Mesocyclogenesis from a theoretical perspective. *The Tornado: Its Structure, Dynamics, Prediction, and Hazards, Geophys. Monogr.*, No 79, Amer. Geophys. Union, 105-114.
- Emanuel, K. A., 1994: *Atmospheric Convection*. Oxford University Press, 580 pp.
- Kessler, E., 1969: On the distribution and continuity of water substance in atmospheric circulations. *Meteor. Monogr.*, No. 32, Amer. Meteor. Soc. 84 pp.
- \_\_\_\_\_, and R. B. Wilhelmson: The simulation of three-dimensional convective storm dynamics. *J. Atmos. Sci.*, **35**, 1070-1096.
- Klemp, J. B. and R. Rotunno, 1983: A study of the tornadic region within a supercell thunderstorm. *J. Atmos. Sci.*, **40**, 359-377.
- Lin, Y. L., R. D. Farley, and H. D. Orville, 1983: Bulk parameterization of the snow field in a cloud model. *J. Climate Appl. Meteor.*, **22**, 1065-1092.
- Markowski, P. M., 2002: Hook echoes and rear-flank downdrafts: A review. *Mon. Wea. Rev.*, **130**, 852-876.
- \_\_\_\_\_, J. M. Straka, and E. N. Rasmussen, 2002: Direct surface thermodynamic observations with the rear-flank downdrafts of nontornadic and tornadic supercells. *Mon. Wea. Rev.*, **130**, 1692-1721.
- \_\_\_\_\_, \_\_\_\_\_, \_\_\_\_\_, 2003: Tornadogenesis resulting from the transport of circulation by a downdraft: Idealized numerical simulations. *J. Atmos. Sci.*, **60**, 795-823.
- Marshall, T. P., 2002: Tornado damage survey at Moore, Oklahoma. *Wea. Forecasting*, **17**, 582-598.
- Rasmussen, E. N., and D. O. Blanchard, 1998: A baseline climatology of sounding-derived supercell and tornado forecast parameters. *Wea. Forecasting*, **13**, 1148-1164.
- Rotunno, R. and J. Klemp, 1985: On the rotation and propagation of simulated supercell thunderstorms. *J. Atmos. Sci.*, **42**, 271-292.
- Skamarock W. C., J. B. Klemp, J. Dudhia, D. O. Gill, D. M. Barker, W. Wang, J. G. Powers, 2005: A description of the advanced research WRF version 2. NCAR Tech. Note. NCAR/TN-468+STR, 88 pp.
- Srivastava, R. C., 1985: A simple model of evaporatively driven downdrafts: Application to microburst downdraft. *J. Atmos. Sci.*, **42**, 1004-1023.
- \_\_\_\_\_, 1987: A model of intense downdrafts driven by the melting and evaporation of precipitation. *J. Atmos. Sci.*, **44**, 1752-1773.
- Thompson, R. E., R. Edwards, J. A. Hart, K. L. Elmore, P. Markowski, 2003: Close proximity soundings within supercell environments obtained from the Rapid Update Cycle. *Wea. Forecasting*, **18**, 1243-1261.
- Weisman, M. L., and J. B. Klemp, 1984: The structure and classification of numerically simulated convective storms in directionally varying wind shears. *Mon. Wea. Rev.*, **112**, 2479-2498.